Adjoint-Based High-Fidelity Aeroelastic Optimization of Wind Turbine Blade for Load Stress Minimization

Evan M. Anderson[1], Faisal Hasan Bhuiyan[2], Dimitri J. Mavriplis[3], and Ray S. Fertig III[4]
University of Wyoming, Laramie, Wyoming, 82071

A high-fidelity multidisciplinary aeroelastic modeling and optimization capability is employed for optimization of structural properties of the 13 meter SWiFT wind turbine blade of Sandia National Laboratories. Both the NSU3D RANS fluid dynamics solver and the AStrO structural finite element solver are developed in-house and validated in previous work. Exact sensitivities of performance objectives are obtained using the adjoint method. For each of several load cases, the composite layup throughout SWiFT blade's internal structure is optimized in order to minimize a scalar stress parameter that has been associated with the propagation of fatigue damage. Three main types of loads regularly experienced by a wind turbine blade are identified: aerodynamic loads, centrifugal loads and gravitational loads. The optimization is performed with the blade under each of these three loads individually, and again with all combined loads present. A 40-60% reduction in the maximum fatigue stress criterion is consistently seen in all cases after optimization.

Nomenclature

A_t, A_s	=	material constants derived from static failure tests of composites
C_{kj}	=	damping matrix in structural dynamic equations
C_{pqrs}	=	4th order material elastic stiffness tensor
D_i	=	set of design variables used to define and modify the properties of a structure
$\bar{f}_g$	=	body force per unit volume in a structure due to gravity
$\bar{f}_c$	=	body force per unit volume in a structure due to centrifugal force
F_k	=	total applied load vector in structural dynamic equations
g	=	acceleration due to gravity
h	=	Plank's constant
$I_{m,t}$	=	invariant of matrix stress in a composite normal to the direction of fiber
I_{ir}	=	3 X 3 identity matrix
k	=	Boltzmann constant
K_{kj}	=	stiffness matrix in structural dynamic equations
L	=	optimization objective function
M_{kj}	=	mass matrix in structural dynamic equations
n	=	parameter quantifying fatigue damage at a point in a material
n_0	=	equilibrium parameter that depends on the damage accumulation exponent
$\bar{r}$	=	normal projection vector from the axis of rotation to a point in a structure
R_k	=	residual vector of the finite element equations governing the behavior of a structure under loading
S_{pqrs}	=	4th order material elastic compliance tensor
t	=	time
t_p^{surf}	=	traction applied over the surface of a structure
U	=	activation energy associated with microcrack accumulation
U_j	=	nodal displacement solution of a structure under deformation

[1] PhD Candidate, email: evanski@uwyo.edu, Member AIAA
[2] PhD Candidate, email: fbhuiyan@uwyo.edu, Member AIAA
[3] Professor, email: mavriplis@uwyo.edu, AIAA Associate Fellow
[4] Assistant Professor, email: rfertig@uwyo.edu, Member AIAA

$\dot{U}_j$ = nodal velocity solution of a structure under deformation
$\ddot{U}_j$ = nodal acceleration solution of a structure under deformation
u = vector displacement of a point in a structure
$\dot{u}_r$ = vector velocity of a point in a structure
$\ddot{u}_r$ = vector acceleration of a point in a structure
v^f = fiber volume fraction of fiber-reinforced composite
$\bar{x}$ = position vector of a point in a structure
α = scalar parameter used in implicit time integration scheme
α_{pr} = 3 X 3 direction cosine transformation matrix
β = scalar parameter used in implicit time integration scheme
γ = activation volume associated with microcrack accumulation
Δt = time step/increment in numerical time integration scheme
ϵ_{pq} = general strain at a point in a structure in vector form
ζ = scalar parameter used in implicit time integration scheme.
λ = damage accumulation exponent
Λ_k = adjoint vector, used to determine gradient of optimization objective
ξ = damping coefficient
ρ = mass density
σ_{pq} = general stress at a point in a structure in vector form
$\sigma_{eff}^{off-axis}$ = effective scalar off-axis stress in the matrix of a composite
$\sigma_{m,ij}$ = tensor components of stress in the matrix of a composite
ϕ_{pj} = matrix of interpolation functions in finite element soloution
ω = angular velocity of a rotating body
Ω = spatial domain of integration

I. Introduction

WIND energy represents an increasingly large portion of the ever-expanding renewable sector. Although there is great potential in wind to sustainably meet global energy needs, numerous challenges still exist which could impede progress in this area. One major concern regarding the economic viability of wind energy is longevity of turbine structures, as they are subject to complex gravitational, centrifugal and aerodynamic loads. These are cyclic in nature and prone to sudden gusts and fluctuations, which can lead to fatigue and failure in both blades and gearboxes. To maximize lifespan of turbine structures it is essential to optimize turbine blade designs to reduce load stresses while still maintaining power output.

Due to their light weight and high strength, wind turbine blades are largely composed of composite materials. One drawback to this in terms of optimizing lifespan is that fatigue behavior in composite materials has long been notoriously difficult to predict.[1, 2] In order to maximize fatigue life, we must identify a means of quantifying the driving force behind fatigue damage. It has been shown that fatigue in fiber-reinforced composites is predominantly matrix-driven, and that the physics of bond-breaking and damage propagation in polymer matrix can be appropriately modeled with the kinetic theory of fracture.[3-7] The *off-fiber-axis* stresses, or shear stresses and normal stresses perpendicular to the fiber direction, are mainly responsible for such damage propagation. Fertig *et al.*[8-10] identified a scalar stress criterion representing the effective off-axis stress in the matrix of a unidirectional fiber composite, and demonstrated its utility as the driving stress in the kinetic theory of fracture. In this study we use this effective off-axis matrix stress as the objective function to be minimized in order to prolong the fatigue life of the SWiFT[11] wind turbine blade of Sandia National Laboratories.

In the field of aerodynamic design and shape optimization, adjoint methods in gradient-based optimization have become mainstream due to their efficiency for problems with many design variables.[12-15] In this study, we utilize gradient optimization with adjoint-based sensitivities to tackle the problem of load stress minimization in turbine blades through optimization of composite layup. In section II we introduce the aeroelastic fluid-structure modeling and optimization capability. In section III we describe the wind turbine blade structural model. In section IV we elaborate on the optimization objective and methodology, and introduce five specific optimization cases. In section V we present the results of our optimizations and in section VI we give conclusions and projections of future work.

II. Aeroelastic Modeling and Optimization Capability

This study utilizes a high-fidelity CFD flow solver and a high-fidelity structural finite element solver, both written in-house for multidisciplinary aeroelastic modeling. The CFD flow solver is NSU3D (Navier-Stokes Unstructured in 3D), which is a widely validated and scalable Reynolds-averaged Navier-Stokes (RANS) solver for unstructured grids. It uses a vertex-centered finite volume formulation, second-order accurate in space and time with a line-implicit multigrid solver. NSU3D has been used in numerous simulations,[13,16-18] and validated through participation in events such as the High-Lift Prediction Workshop.[16]

The structural finite element solver is AStrO (Adjoint-based Structural Optimizer), developed over the last three years and demonstrated in previous work.[17,18] AStrO supports linear and nonlinear finite element modeling of 3D solid continuum and shell structures. Dynamic systems can be modeled with implicit second-order accurate time integration by the Hilbur-Huges-Taylor "alpha" method,[19] and processing of model input files generated by Abaqus[20] commercial finite element software is supported.

NSU3D and AStrO are capable of running tightly coupled analysis through a fluid-structure interface[17]. Each point in the CFD grid adjacent to the surface of the structural finite element mesh is initially projected to its nearest point on the structural surface, and hence imperfectly matching fluid and structural grids can be accomodated. In addition, NSU3D is capable of deforming its grid to adapt to structural displacements using a linear elastic displacement analogy. Each time step of a simulation, NSU3D solves for the aerodynamic loads given the current structural displacement, and passes those loads to AStrO through the interface mapping. AStrO then updates the structural displacement given the loads, and passes those displacements back though the interface. The process is repeated until the state at the next time step converges.

Both NSU3D and AStrO are built with the capability for obtaining exact sensitivities of solution-derived objectives with respect to customized design parameters using the adjoint method. With the use of the adjoint, only one adjoint solution is required on each optimization design cycle regardless of the number of design parameters,[12-14] enabling efficient gradient-based optimization for any number of parameters.

In the present study, NSU3D and AStrO are used in the tightly-coupled simulation process described above to generate realistic steady-state aerodynamic loads applied to the SWiFT[11] wind turbine blade model described in section III. These aerodynamic loads are retained and considered constant throughout the process of a purely structural optimization, executed by AStrO alone. Future works will incorporate both capabilities into fully-coupled optimization studies.

In gradient optimization, an objective quantity L to be optimized is defined as a function of a set of design variables D_i, as well as a set of solution variables U_j that define the physical response of a system.

$$L = L\left(D_i, U_j(D_i)\right) \tag{1}$$

The objective function is optimized by stepping through a series of iterations in which the design variables are incremented in a step direction determined by the gradient of L with respect to D_i. From differentiation of Eq. (1), the gradient of L is

$$\frac{dL}{dD_i} = \frac{\partial L}{\partial D_i} + \frac{\partial L}{\partial U_j}\frac{\partial U_j}{\partial D_i} \tag{2}$$

The solution variables must always satisfy the appropriate set of governing equations,

$$R_k\left(D_i, U_j(D_i)\right) = 0 \tag{3}$$

Differentiating Eq. (3), we have

$$\frac{dR_k}{dD_i} = \frac{\partial R_k}{\partial D_i} + \left[\frac{\partial R_k}{\partial U_j}\right]\frac{\partial U_j}{\partial D_i} = 0 \Longrightarrow \frac{\partial U_j}{\partial D_i} = -\left[\frac{\partial R_j}{\partial U_k}\right]^{-1}\frac{\partial R_k}{\partial D_i} \tag{4}$$

We can then re-write Eq. (2) as

$$\frac{dL}{dD_i} = \frac{\partial L}{\partial D_i} - \frac{\partial L}{\partial U_j}\left[\frac{\partial R_j}{\partial U_k}\right]^{-1}\frac{\partial R_k}{\partial D_i} \tag{5}$$

The most computationally expensive step in evaluating Eq. (5) is the solution of the linear system to apply the inverse matrix operation. But the partial derivative of L with respect to U_j does not depend on D_i, so if we first evaluate the *adjoint*, Λ_k by solving

$$\left[\frac{\partial R_k}{\partial U_j}\right]\Lambda_k = \frac{\partial L}{\partial U_j} \tag{6}$$

and then evaluate

$$\frac{dL}{dD_i} = \frac{\partial L}{\partial D_i} - \Lambda_k \frac{\partial R_k}{\partial D_i} \tag{7}$$

then we only need to solve one linear system (Eq. (6)) to get the gradient of the objective with respect to any number of design variables. Note that Eq. (6) and (7) are in index notation, and the adjoint is solved with the transpose Jacobian of the discretized governing equations.

Since the present study involves structural optimization, the solution variables in this case are structural nodal displacements, and the governing equations are finite element equations, derived from the principle of virtual work.[21] The general statement of the principle of virtual work for a structural dynamic system is as follows:

$$\int_\Omega \sigma_{pq}\delta\epsilon_{pq}d\Omega + \int_\Omega \xi\dot{u}_p\delta u_p d\Omega + \int_\Omega \rho\ddot{u}_p\delta u_p d\Omega - \int_\Omega f_p\delta u_p d\Omega - \int_\mathrm{A} t_p^{surf}\delta u_p d\mathrm{A} = 0 \tag{8}$$

In the above u_p, $\dot{u}_p$ and $\ddot{u}_p$ are the vector displacement, velocity and acceleration at a point in a structure, σ_{pq} and ϵ_{pq} are the stress and strain in second-order tensor form, ξ is the damping coefficient, ρ is the mass density, f_p is applied body force per unit volume, and t_p^{surf} is applied surface traction per unit area on the structure. The δ operator indicates a *variation* on the function to its right, meaning the above must hold for any variation of the displacement field u_p. The final term is an integral of traction applied over the surface area of the structure, while all other terms are volume integrals over the body of the structure. Let us first consider the steady-state case, in which velocity and acceleration are zero. Eq. (8) then reduces to

$$\int_\Omega \sigma_{pq}\delta\epsilon_{pq}d\Omega - \int_\Omega f_p\delta u_p d\Omega - \int_\mathrm{A} t_p^{surf}\delta u_p d\mathrm{A} = 0 \tag{9}$$

In finite element analysis, the displacement solution is assumed to take the form

$$u_p = \phi_{pj}(x_q)U_j \tag{10}$$

where ϕ_{pj} is a matrix of known spatial interpolation functions (or basis functions), and U_j is the discrete set of solution variables, in this case element nodal displacements, to be determined by the governing equations. By extension we can define strain in terms of the gradients of displacement. AStrO supports the use of nonlinear strain definitions, accommodating large deflections in the structure, but for the present work our studies are limited to the linear definition of strain,

$$\epsilon_{pq} = \frac{1}{2}\left(\frac{\partial u_p}{\partial x_q} + \frac{\partial u_q}{\partial x_p}\right) = \frac{1}{2}\left(\frac{\partial \phi_{pj}}{\partial x_q} + \frac{\partial \phi_{qj}}{\partial x_p}\right)U_j \tag{11}$$

We also presently assume linear elastic material behavior, meaning strain maps to stress with a material stiffness tensor, C_{pqrs}, which is independent of deformation as follows

$$\sigma_{pq} = C_{pqrs}\epsilon_{rs} \tag{12}$$

The first term in Eq. (9), representing the elastic stiffness of the structure is invariant with respect to the coordinate system in which the stress and strain are defined. It is convenient, and therefore common practice to define strain at each section of a structure in a coordinate system that aligns with the local material axes of symmetry. We follow this practice in the present work, denoting strain in the local material coordinate system ϵ^L_{pq}, which relates to strain in the global coordinate system, ϵ_{rs} as follows

$$\epsilon^L_{pq} = \alpha_{pr}\alpha_{qs}\epsilon_{rs} \tag{13}$$

α_{pr} represents the direction cosine transformation matrix that maps a tensor between the global and local coordinate systems. The stress in the local coordinate system can then be found as

$$\sigma^L_{pq} = C^L_{pqrs}\epsilon^L_{rs} \tag{14}$$

In variational calculus, variation functions follow chain-rule differentiation, so if we have a function Ψ of a set of discrete parameters U_k, then

$$\delta\Psi(U_k) = \frac{\partial\Psi}{\partial U_k}\delta U_k \tag{15}$$

By this we can re-write the variations of displacement and strain assuming the discretized solution,

$$\delta u_p = \frac{\partial u_p}{\partial U_k}\delta U_k = \phi_{pk}\delta U_k \tag{16}$$

$$\delta\epsilon_{pq} = \frac{\partial\epsilon_{pq}}{\partial U_k}\delta U_k = \frac{1}{2}\left(\frac{\partial\phi_{pk}}{\partial x_q} + \frac{\partial\phi_{qk}}{\partial x_p}\right)\delta U_k \tag{17}$$

$$\delta\epsilon^L_{pq} = \frac{\partial\epsilon^L_{pq}}{\partial U_k}\delta U_k = \alpha_{pr}\alpha_{qs}\frac{1}{2}\left(\frac{\partial\phi_{rk}}{\partial x_s} + \frac{\partial\phi_{sk}}{\partial x_r}\right)\delta U_k \tag{18}$$

Substituting the discrete form of the variations of displacement and strain into Eq. (9), we have

$$\left\{\frac{1}{4}\left[\int_\Omega \alpha_{pr}\alpha_{qs}\left(\frac{\partial\phi_{rk}}{\partial x_s} + \frac{\partial\phi_{sk}}{\partial x_r}\right)C^L_{pqtu}\alpha_{tv}\alpha_{uw}\left(\frac{\partial\phi_{vj}}{\partial x_w} + \frac{\partial\phi_{wj}}{\partial x_v}\right)d\Omega\right]U_j - \int_\Omega f_p\phi_{pk}d\Omega - \int_\mathrm{A} t_p^{surf}\phi_{pk}d\mathrm{A}\right\}\delta U_k = 0 \tag{19}$$

Because the variation of the solution parameters δU_k appears in every term of the equation, and these parameters are not functions of space, it can be factored out of the whole expression as seen in Eq. (19). Again the above must hold for *any* variation of the solution parameters, and therefore the expression in brackets must be zero. This gives us our discretized governing equations for static displacement, in Eq. (20).

$$R_k = \frac{1}{4}\left[\int_\Omega \alpha_{pr}\alpha_{qs}\left(\frac{\partial\phi_{rk}}{\partial x_s} + \frac{\partial\phi_{sk}}{\partial x_r}\right)C^L_{pqtu}\alpha_{tv}\alpha_{uw}\left(\frac{\partial\phi_{vj}}{\partial x_w} + \frac{\partial\phi_{wj}}{\partial x_v}\right)d\Omega\right]U_j - \int_\Omega f_p\phi_{pk}d\Omega - \int_\mathrm{A} t_p^{surf}\phi_{pk}d\mathrm{A} = 0 \tag{20}$$

The residual vector of the discretized equations in Eq. (20) is a function of both the displacement solution U_j and the design variables D_i defining a structure. Stress and strain are inherently functions of displacement, and in some cases, such as coupled fluid-structural simulations, applied loads can vary with displacement as well. However, for the scope of this work we will assume the applied loads to be constant with respect to displacement. Therefore, the Jacobian of the governing equations with respect to displacement solution variables can be expressed

$$\left[\frac{\partial R_k}{\partial U_j}\right] = \frac{1}{4}\int_\Omega \alpha_{pt}\alpha_{qu}\left(\frac{\partial\phi_{tk}}{\partial x_u} + \frac{\partial\phi_{uk}}{\partial x_t}\right)C^L_{pqrs}\alpha_{rv}\alpha_{sw}\left(\frac{\partial\phi_{vj}}{\partial x_w} + \frac{\partial\phi_{wj}}{\partial x_v}\right)d\Omega \tag{21}$$

Design variables in general can affect the material stiffness tensor C^L_{pqrs}, the size and shape of structural elements, which determine the gradient of the interpolation matrix $\frac{\partial\phi_{pj}}{\partial x_q}$, and the local material coordinate system, which determines the local transformation matrix α_{pq}. In the optimizations for the present study, we consider only

design variables that affect local material coordinate system, or α_{pq}. Under such circumstances, differentiating Eq. (20) by D_i yields

$$\frac{\partial R_k}{\partial D_i} = \frac{1}{2}\int_\Omega \left(\frac{\partial \sigma_{pq}^L}{\partial D_i} \alpha_{pr}\alpha_{qs} \left(\frac{\partial \phi_{rk}}{\partial x_s} + \frac{\partial \phi_{sk}}{\partial x_r} \right) + C_{pqrs}^L \alpha_{rt}\alpha_{su} \left(\frac{\partial \phi_{tk}}{\partial x_u} + \frac{\partial \phi_{uk}}{\partial x_t} \right) \frac{\partial}{\partial D_i} \left(\frac{\partial \epsilon_{pq}^L}{\partial U_k} \right) \right) d\Omega \tag{22}$$

where

$$\frac{\partial \sigma_{pq}^L}{\partial D_i} = \frac{1}{2} C_{pqrs}^L \left(\frac{\partial \alpha_{rt}}{\partial D_i} \alpha_{su} + \alpha_{rt} \frac{\partial \alpha_{su}}{\partial D_i} \right) \left(\frac{\partial \phi_{tj}}{\partial x_u} + \frac{\partial \phi_{uj}}{\partial x_t} \right) U_j \tag{23}$$

$$\frac{\partial}{\partial D_i} \left(\frac{\partial \epsilon_{pq}^L}{\partial U_k} \right) = \frac{1}{2} \left(\frac{\partial \alpha_{pr}}{\partial D_i} \alpha_{qs} + \alpha_{pr} \frac{\partial \alpha_{qs}}{\partial D_i} \right) \left(\frac{\partial \phi_{rk}}{\partial x_s} + \frac{\partial \phi_{sk}}{\partial x_r} \right) \tag{24}$$

On each design cycle in the optimization process, the solution for nodal displacements is first found by solving Eq. (25) for U_j.

$$\left[\frac{\partial R_k}{\partial U_j} \right] U_j = -R_k \tag{25}$$

Since in the present study we assume small displacements (linear geometry), $\left[\frac{\partial R_k}{\partial U_j} \right]$ is a constant matrix with respect to U_j, forming a linear system. Eq. (25) is often denoted

$$[K_{kj}]U_j = F_k \tag{26}$$

This enables us to evaluate the objective function, as further explained in section IV. The adjoint is then found using Eq. (6) and (21) and finally the gradient of the objective function is evaluated using Eq. (7) and (22).

For dynamic problems, we use an implicit time integration scheme to obtain the displacement solution at each of a series of time steps throughout the period of interest. Following a similar process as for the steady-state equations, the discretized form of virtual work for a dynamic system at a moment in time is

$$R_k = \frac{1}{4}\left[\int_\Omega \alpha_{pr}\alpha_{qs} \left(\frac{\partial \phi_{rk}}{\partial x_s} + \frac{\partial \phi_{sk}}{\partial x_r} \right) C_{pqtu}^L \alpha_{tv}\alpha_{uw} \left(\frac{\partial \phi_{vj}}{\partial x_w} + \frac{\partial \phi_{wj}}{\partial x_v} \right) d\Omega\right] U_j + \int_\Omega \xi \phi_{pk}\phi_{pj} d\Omega\, \dot{U}_j + \int_\Omega \rho \phi_{pk}\phi_{pj} d\Omega\, \ddot{U}_j$$

$$- \int_\Omega f_p \phi_{pk} d\Omega - \int_\mathrm{A} t_p^{surf} \phi_{pk} d\mathrm{A} = 0 \tag{27}$$

Eq. (27) is often denoted

$$R_k = [K_{kj}]U_j + [C_{kj}]\dot{U}_j + [M_{kj}]\ddot{U}_j - F_k = 0 \tag{28}$$

The Hilbur-Huges-Taylor "alpha" method[19] of time-integration is used, such that the governing equations for each time step, with the step denoted by the superscript N, are as follows

$$R_k^N = (1+\alpha)\left\{[K_{kj}]U_j + [C_{kj}]\dot{U}_j + -F_k\right\}^N - \alpha\left\{[K_{kj}]U_j + [C_{kj}]\dot{U}_j + -F_k\right\}^{N-1} + [M_{kj}]\ddot{U}_j^N = 0 \tag{29}$$

The velocity $\dot{U}_r$ and acceleration $\ddot{U}_r$ at any point in the structure are defined by the Newmark Beta[19] series expansions as follows:

$$U_r^N = U_r^{N-1} + \Delta t \dot{U}_r^{N-1} + \frac{\Delta t^2}{2}\left((1-2\beta)\ddot{U}_r^{N-1} + 2\beta \ddot{U}_r^N \right) \tag{30}$$

$$\dot{U}_r^N = \dot{U}_r^{N-1} + \Delta t\left((1-\zeta)\ddot{U}_r^{N-1} + \zeta\ddot{U}_r^N\right) \tag{31}$$

In Eq. (29), (30) and (31), α, β and ζ are weighting parameters set within the following ranges:

$$\begin{aligned} -1 < \alpha \leq 0 \\ 0 < \beta \leq 0.5 \\ 0 < \zeta \leq 1 \end{aligned} \tag{32}$$

The above time integration scheme can be set to be both unconditionally stable, and second-order accurate in time. Modifying the parameters in Eq. (32) control aspects like numerical dissipation, stability and accuracy, making it a versatile method. On a dynamic time step, the Jacobian matrix is expressable as

$$\left[\frac{\partial R_k^N}{\partial U_j^N}\right] = (1+\alpha)([K_{kj}] + \frac{\zeta}{\Delta t\beta}[C_{kj}]) + \frac{1}{\beta\Delta t^2}[M_{kj}] \tag{33}$$

The displacement solution at each time step can then be found by solving

$$\left[\frac{\partial R_k^N}{\partial U_j^N}\right] U_j = -R_k^N \tag{34}$$

using the solution for displacement, velocity and acceleration at the previous time step. Velocity and acceleration at the current time step can then be updated using Eq. (30) and (31).

The optimization process for dynamic simulations is fundamentally the same as for steady-state cases, except that the displacement solution and adjoint must be found at every individual time step. $\frac{\partial R_k}{\partial D_i}$ can still be evaluated as described in Eq. (22) for the steady-state case. On each optimization design cycle, the displacement history is solved for given the current values of the design variables using Eq. (34) and written to disk for each time step. Then for each time step in reverse order (due to the fact that the adjoint is found from the transpose of the global system), the adjoint is calculated using Eq. (6), and the gradient, or sensitivity of the objective function with respect to each design variable at that time step is evaluated from Eq. (7). After all time steps are completed, we have the total gradient of the objective function at that design cycle, and we can proceed with the optimization.

III. Structural Model of Sandia SWiFT 13 meter Wind Turbine Blade

The wind turbine blade model used as the subject for this work is a 13 meter blade with a 0.6 meter cylindrical section diameter from Sandia National Laboratories used for the SWiFT project[11]. For this model detailed geometric and material composition data is readily available, and previous work has been done by Bhuiyan *et al.*[22] in generating the model in Abaqus for conducting fatigue studies. The blade's outer skin geometry is constructed by lofting together a series airfoil cross-sections defined at each of 34 stations along the spanwise length. The cross-section at outboard stations consists of leading edge and trailing edge panels, and a central box beam with thick reinforced spar caps on the upper and lower sides and shear webs connecting the spar caps running normal to the chord. Figure 1 illustrates the general blade geometry.

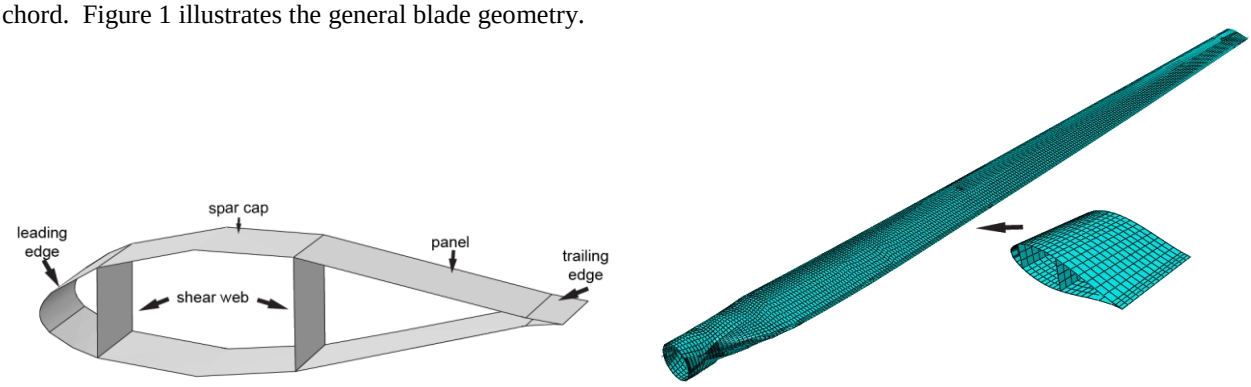

Figure 1. Cross-sectional design and spanwise geometry of SWiFT wind turbine blade (Ref. 22).

The finite element mesh for the model was generated in Abaqus out of 16,310 4-node shell elements, following the definition of each spanwise station cross-section from the SWiFT report[11]. Originally, the blade structure was divided into 388 sections, each with a composite layup definition made from an assortment of materials, as illustrated in Figure 2. For the present studies, the entire blade structure is considered to be a made from UD1200 glass-fiber reinforced polyester resin laminate, with each individual element composed of a single ply with a unique fiber orientation, further explained in the following section.

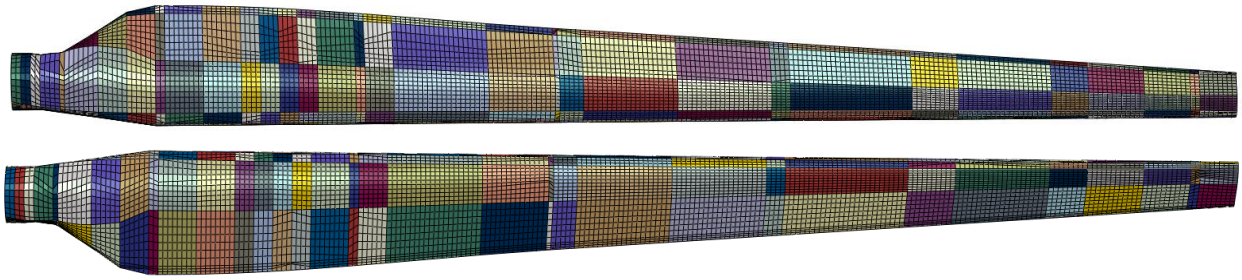

Figure 2. Section divisions of the SWiFT wind turbine blade originally defined by the structural finite element model.

In their previous work, Bhuiyan *et al.*[22] used a scalar effective off-axis matrix stress as the driving force of composite fatigue damage in their model based on the kinetic theory of fracture. The effective off-axis matrix stress is defined as[22]

$$\sigma_{eff}^{off-axis} = \sqrt{A_t\{I_{m,t}\}^2 + \sigma_{m,12}^2 + \sigma_{m,13}^2 + A_s(\tfrac{1}{4}(\sigma_{m,22} - \sigma_{m,33})^2 + \sigma_{m,23}^2)} \tag{35}$$

Here A_t and A_s are material parameters obtained from static failure tests of a particular composite. $I_{m,t}$ is an invariant derived from the components of matrix stress normal to the fiber direction. Macaulay brackets {} indicate that the term becomes zero if the quantity inside is negative. In the present application of the kinetic theory of fracture, a damage parameter, n, is used to quantify the accumulation of microcracking and fatigue damage at a point in a material. The above effective off-axis stress parameter is used to calculate the rate of damage accumulation as follows[22]:

$$\frac{dn}{dt} = (n_0 - n)^{\lambda} \frac{kT}{h} \exp\left(\frac{\gamma \sigma_{eff}^{off-axis} - U}{kT}\right) \tag{36}$$

In Eq. (36) λ is a damage accumulation exponent, U is an activation energy associated with microcracking, and γ is an activation volume associated with microcracking, all material-dependent. T is absolute temperature, h is Plank's constant and k is Boltzmann's constant. By integrating the damage parameter throughout the structure over cyclic loading history, we can perform progressive fatigue failure analysis and predict the life of the structure. The off-axis stress components in Eq. (35) refer to volume-averaged constituent-level stresses in the matrix of the composite, not the overall macroscopic composite stress. Matrix stresses in a composite are obtained from structural stresses in the finite element analysis using multi-continuum theory (MCT)[23-24], a widely validated technique developed at the University of Wyoming for extracting constituent stresses in heterogeneous materials. If the elastic material properties are known for a composite as a whole, as well as for the fiber and matrix as individual constituents, and the fiber volume fraction v^f is also known, then the volume-averaged stresses for fiber $\sigma_{f,ij}$ and matrix $\sigma_{m,ij}$ can be obtained from composite stress $\sigma_{c,ij}$ through the following equations:

$$(1 - v^f)\sigma_{m,ij} + v^f \sigma_{f,ij} = \sigma_{c,ij} \tag{37}$$

$$(1 - v^f)S_{m,ijkl}\sigma_{m,kl} + v^f S_{f,ijkl}\sigma_{f,kl} = S_{c,ijkl}\sigma_{c,kl} \tag{38}$$

Here $S_{m,ijkl}$, $S_{f,ijkl}$, and $S_{c,ijkl}$ are the material compliance tensors, or the inverse stiffness tensors for matrix, fiber, and composite respectively. Combining Eq. (36) and (37) to eliminate the fiber stress gives us a relationship between composite stress and matrix stress

$$\sigma_{m,ij} = \frac{1}{(1-vf)}\left[I_{ir}I_{js} - C_{f,ijpq}S_{m,pqrs}\right]^{-1}\left[I_{rk}I_{sl} - C_{f,rspq}S_{c,pqkl}\right]\sigma_{c,kl} \tag{39}$$

I_{ir} is the 3 X 3 identity matrix, and $C_{f,ijpq}$ is the material stiffness tensor for the fiber. The composite stress in a structure is calculated using the finite element displacement and strain solution (using Eq. (14)). From this we can obtain the necessary matrix stresses from Eq. (39), and calculate the effective off-axis stress from Eq. (35).

IV. Optimization Objective and Methodology

Based on the established model from the kinetic theory of fracture in Eq. (36), minimization of the effective off-axis stress in Eq. (35) should impede the progression of fatigue damage, and maximize the lifespan of the structure. Specifically, we define our scalar objective function, L to be the 4th power of the effective off-axis stress, integrated in space and time,

$$L = \int_0^t \int_\Omega \left(\sigma_{eff}^{off-axis}\right)^4 d\Omega dt \tag{40}$$

By using the 4th power we target the regions of highest effective stress in the blade, prioritizing those regions in the optimization. We minimize the objective in Eq. (40) by tailoring the composite ply orientations. Specifically, each design variable represents the angle of rotation of the composite fiber direction about the local z-axis of a structural element, with respect to its original orientation. The local z-axis of shell element is always defined normal to the element's midplane, and therefore the fiber direction always stays within the midplane of the shell. A given design variable D_i defines the material local coordinate system for the i^{th} element as follows

$$\alpha_{pq}^{i}(D_i) = \begin{bmatrix} \cos(D_i) & \sin(D_i) & 0 \\ -\sin(D_i) & \cos(D_i) & 0 \\ 0 & 0 & 1 \end{bmatrix}_{pr} \alpha_{rq}^{i,0} \tag{41}$$

where $\alpha_{rq}^{i,0}$ is the initial coordinate system transformation matrix for element i, aligning the fiber direction in the global z-direction (see Figure 3) projected onto the element midplane. Eq. (41) is used to obtain the displacement solution, as well as the objective gradient by incorporating α_{pq}^{i} and $\frac{\partial \alpha_{pq}^{i}}{\partial D_i}$ into Eq. (22), (23) and (24).

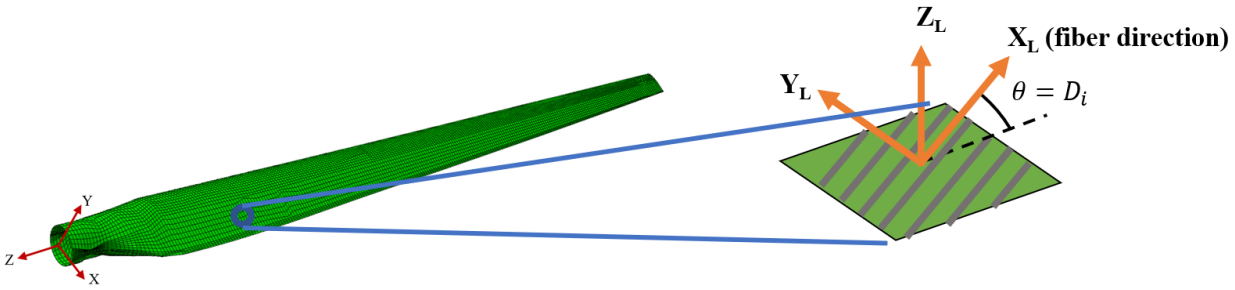

Figure 3. Stuctural-level and element level local coordinate systems for SWiFT blade model.

One of the greatest advantages to using the adjoint method to obtain objective sensitivities in gradient optimization is the near independence of the cost of calculating sensitivities to the number of design variables. That is, for the cost of one steady-state/dynamic simulation, the sensitivities of the objective with respect to any number of design variables can be obtained, as explained in section II. We utilize that power here by allowing every individual element in the entire structural mesh to have its own composite ply orientation, optimized for the state of stress at that particular point. This makes a total of 16,310 design variables, one for each element in the structure.

The optimization algorithm used is a steepest descent backtracking line search[25], using the gradient of the objective function obtained using the adjoint method as the search direction at each design cycle. As described in

section II, each design cycle involves first solving for the structural displacements at the current values of the design variables, then solving for the adjoint and calculating the gradient of the objective function with respect to the design variables. Solutions of linear systems are performed with a direct solver built into AStrO. The size of the structural finite element model in this case is such that the optimizations can be run on a single desktop Linux machine, running about 30 seconds per design cycle per time step in the solution domain. For all the present studies, the optimizer runs through ten design cycles for each design problem.

An important consideration is that the optimum ply orientation layup for the structure will inevitably depend on loading. Wind turbines are routinely subject to three main types of applied loads: 1) aerodynamic loads 2) gravitational loads and 3) centrifugal loads. In this work we perform the optimization analysis with each type of of loading individually before examining the total combined loading to compare their contributions to the results. We investigate a total of five load cases, detailed in the following sections.

1. Steady-State Analysis Under Centrifugal Loading Only

The first load case subjects the turbine blade to centrifugal loads only. The structural response of the blade is analyzed by AStrO in a coordinate system rotating with the blade with its y-axis as the axis of rotation. The x-axis runs in the blade's general chord direction and the z-axis runs parallel with the longitudinal axis of the blade, as shown in Figure 3. Under such conditions the centrifugal loads can be modeled as a static body force distributed throughout the structure. The body force per unit volume due to centrifugal loading is constant in time at any point in the structure, since the angular velocity is assumed constant, and is calculated by

$$\bar{f}_c = \rho\omega^2\bar{r}(\bar{x}) \tag{42}$$

where ρ is the mass density of the material at a point in the structure, ω is the angular velocity of the rotating blade, and $\bar{r}$ is the normal position vector projected from the axis of rotation (y-axis) to the point, or

$$\bar{r}(\bar{x}) = [x_c, 0, z_c] \tag{43}$$

The angular velocity is set to correspond with the optimal rate for power production for this particular turbine, or 43 rpm.

2. Dynamic Analysis Under Gravitational Loads Only

The second load case subjects the blade to gravitational loads only. In the local rotating frame of motion, the gravitational component of the body force is constant in magnitude at a given point on the structure, but its direction varies cyclically with a frequency matching the angular velocity of the blade. For this component,

$$\bar{f}_g = \rho g\bar{n}(t) \tag{44}$$

where g is the acceleration due to gravity, and the unit vector $\bar{n}$ varies in time as follows:

$$\bar{n}(t) = [\sin(\omega t), 0, -\cos(\omega t)] \tag{45}$$

Because of the load's dependence on time, this case must be analyzed dynamically. The structure is started from rest, with both displacement and velocity at zero. Under such conditions there can be an initial transient period before the structure settles into its periodic response. Therefore, the blade is rotated through three full revolutions under the load field defined in Eq. (44) to more thoroughly capture the range of motion. The optimization is performed based on the stress response integrated over the entire time period.

3. Steady-State Analysis Under Aerodyamic Loads Only

The third load case subjects the blade to aerodynamic loads only. Aerodynamic loads on the blade structure are pre-generated by the NSU3D flow solver, by solving for the pressure distribution and skin friction over the blade surface assuming an inflow wind velocity of 12 meters per second, as described in section II. In reality, these aerodynamic loads are time-varying, but in this case we take them to be constant throughout the optimization

process, corresponding to the steady-state solution under these conditions. We then perform the optimization based on the steady-state response under these loads.

4. Steady-State Analysis Under Combined Loading

The fourth load case subjects the blade to centrifugal, gravitational and aerodynamic loads combined, with the gravitational load in Eq. (44) evaluated at $\omega t = \pi/2$. That is, with the gravitational load purely in the direction normal to the blade axis, corresponding to the blade in the horizontal position. In this position the bending loads due to gravity are maximized, as are the maximum stresses in the structure. The optimization is then performed based on the static response under these loads.

5. Dynamic Analysis Under Combined Loading

In the fifth and final load case, we again apply all three types of loads simultaneously, but simulate the full dynamic response of the structure. We account for the time-dependence of the gravitational loads, but still consider the aerodynamic loads to be constant, corresponding to the steady state solution as with load case 3. Again we run the analysis through three full revolutions.

Three of the five of the above load cases are run as steady-state simulations, which may seem inappropriate since fatigue is an inherently time-dependent phenomenon. However, fatigue analysis often assumes a given load distribution with a periodically varying amplitude. Under this assumption, the maximum stress in a steady state response can be used to estimate fatigue life.

V. Optimization Results

For all of the load cases described in the previous section, we perform the optimization analysis, keeping track of three key quantities at each design cycle: 1) the value of the objective function, 2) the root-mean-square of the objective gradient, and 3) the maximum value of the effective off-axis matrix stress encountered by any point in the structure at any moment in the time history. The progression of all these quatities, non-dimensionalized by their initial values can be seen in Figures 4 and 5.

Although the optimized ply configuration is different for each load case, the optimization consistently reduces the maximum effective off-axis matrix stress by about 40-60%. Table 1 shows the change in the maximum effective off-axis matrix stress for each of the five load cases.

Table 1. Maximum effective off-axis matrix stress in SWiFT blade structure before and after optimization.

Load Case	Max. Stress Before Opt. (MPa)	Max. Stress After Opt. (MPa)	Percent Reduction
Steady-State, Centrifugal	15.39	6.245	59.41%
Dynamic, Gravitational	17.10	7.610	55.49%
Steady-State, Aerodynamic	17.64	10.18	42.30%
Steady-State, Combined	26.90	12.35	54.08%
Dynamic, Combined	31.08	15.20	51.11%

To estimate the corresponding effect on fatigue life, we consult S-N fatigue data for E-glass/epoxy published by Hashin and Rotem[1]. Figure 6 shows a logarithmic plot of stress versus number of cycles to failure for the published data points, along with a trendline fit to the data.

For the present puposes, the trend in Figure 6 is qualitative since the state of stress represented by the data does not match that in every point thoughout the SWiFT blade structure. Nevertheless it is clearly evident that the amount of off-axis stress reduction shown in Figures 4 and 5 has great potential to impact the number of cycles to failure. In the final case of dynamic simulation under combined loading, for example, our optimization brought the maximum effective off-axis stress from 31 MPa down to 15 MPa. Although these values do not fall within the range of the data set, the trend of the data would indicate an increase in the number cycles to failure by several orders of magnitude.

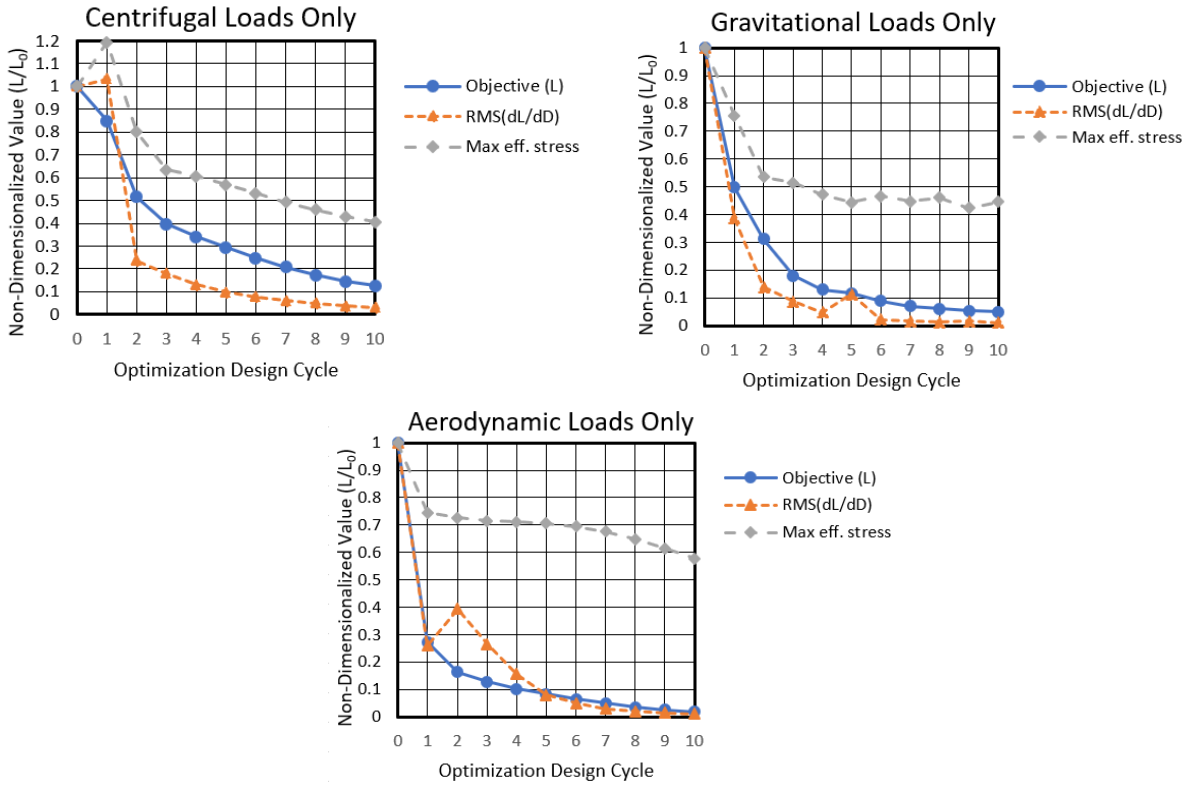

Figure 4. Optimization history for individual loading conditions on the SWiFT turbine blade.

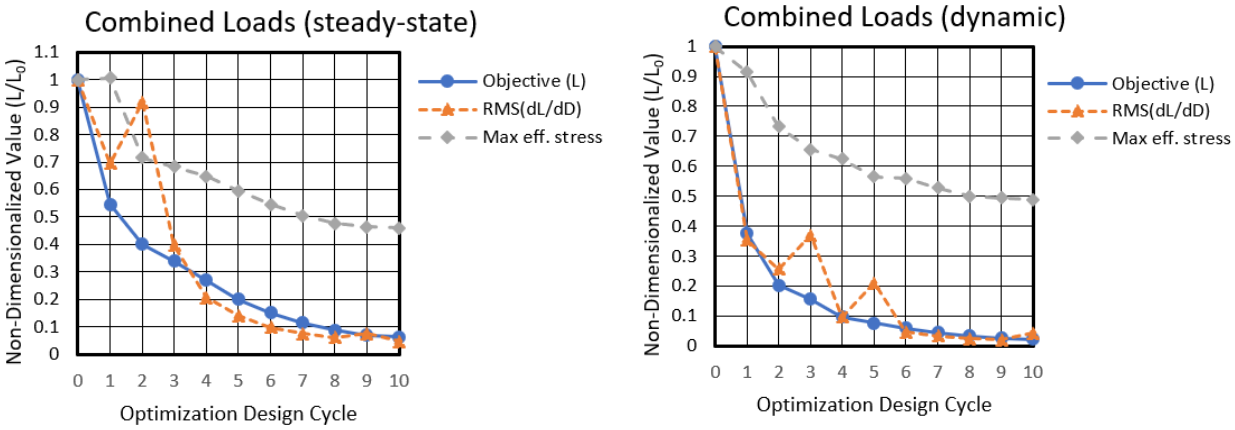

Figure 5. Optimization history for combined loading conditions on the SWiFT turbine blade.

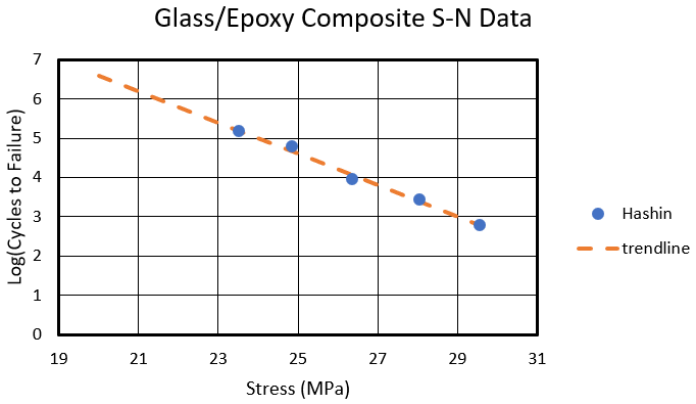

Figure 6. Published S-N data for E-glass epoxy composite (Ref. 1), loaded at 60º from fiber direction with corresponding trendline.

To weigh the relative contributions of each type of loading, we can compare the final optimized ply angles for each element between the different cases. We use the final load case, incorporating all loads in dynamic simulation, as a benchmark of comparison for the others, as it is presumably the most realistic simulation of what a turbine blade experiences. In Table 2, we compare the 2-norm of the difference between the optimized ply angles of each element for the final load case with each of the previous load cases. The smaller the value of the norm, the smaller the difference and the closer the overall agreement in the optimized ply configurations with the final combined load case.

Table 2. Comparison of final optimized ply angles between final load case, and all previous load cases.

	Centrifugal Only (steady-state)	**Gravitational Only (dynamic)**	**Aerodynamic Only (steady-state)**	**All Loads (steady-state)**
$\left\|\boldsymbol{D_i} - \boldsymbol{D}_{i,final\ case}\right\|_2$	773.2º	973.2º	534.9º	398.4º

This metric would indicate that under the conditions assumed in this case, aerodynamic loading has the strongest influence on the optimum ply configurations of the three main types of loading. The configuration for the static analysis under combined loading shows the closest agreement of all, implying that a reasonable solution could perhaps be obtained from a static approximation of a dynamic problem. The same observations can be seen qualitatively from the spatial plots of angle change and effective off-axis matrix stress in Figures 7-11.

One potential concern for the present optimization approach is that it may not be practical from a fabrication point of view to allow each structural finite element's representative fragment on the blade to have its own unique ply configuration. However, the results may still teach us valuable information that could be utilized within the confines of fabrication.

Two key observations can be taken from Figures 7-11. First, the vast majority of elements in the structure had very little change in their ply angle due to optimization, less than 1º change. The most affected areas are concentrated near the root of the blade, which is intuitive since these are the areas of highest stress for a structure under primarily bending loads. Second, elements of similar angle change tend to cluster together in groups, since neighboring elements tend to experience similar states of stress under a given loading.

The implication from these observations is that if a blade were to be fabricated to accommodate optimizations such as these, it would likely be only a few regions that would need special customization of ply orientations. Also the sections of the most affected areas could be defined to encompass elements of similar ply orientation, and each section given a homogenized ply configuration, resulting in relatively few specifically tailored regions. Alternatively, further optimizations could be conducted using ply orientation design variables that affect pre-determined regions or groups of elements in the finite element model.

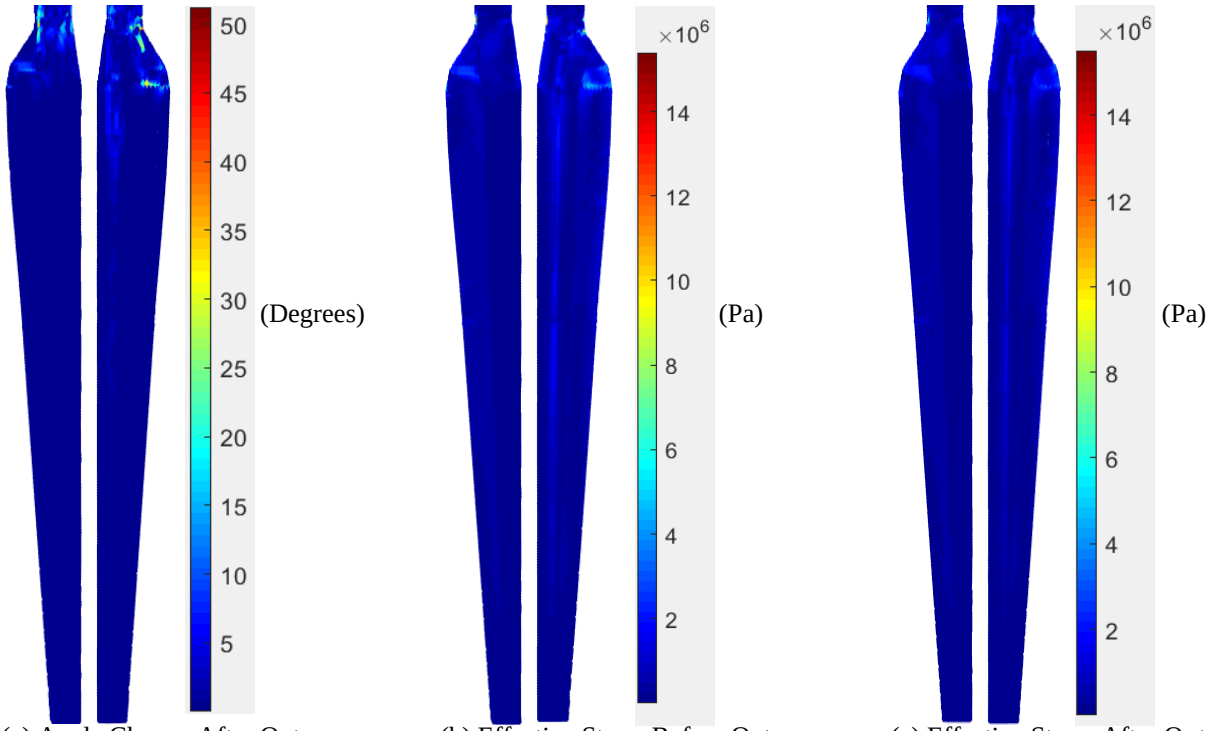

(a) Angle Change After Opt. (b) Effective Stress Before Opt. (c) Effective Stress After Opt.

Figure 7. Spatial distribution of local composite ply angle change and effective off-axis matrix stress before and after optimization for steady-state optimization subject to centrifugal loads only.

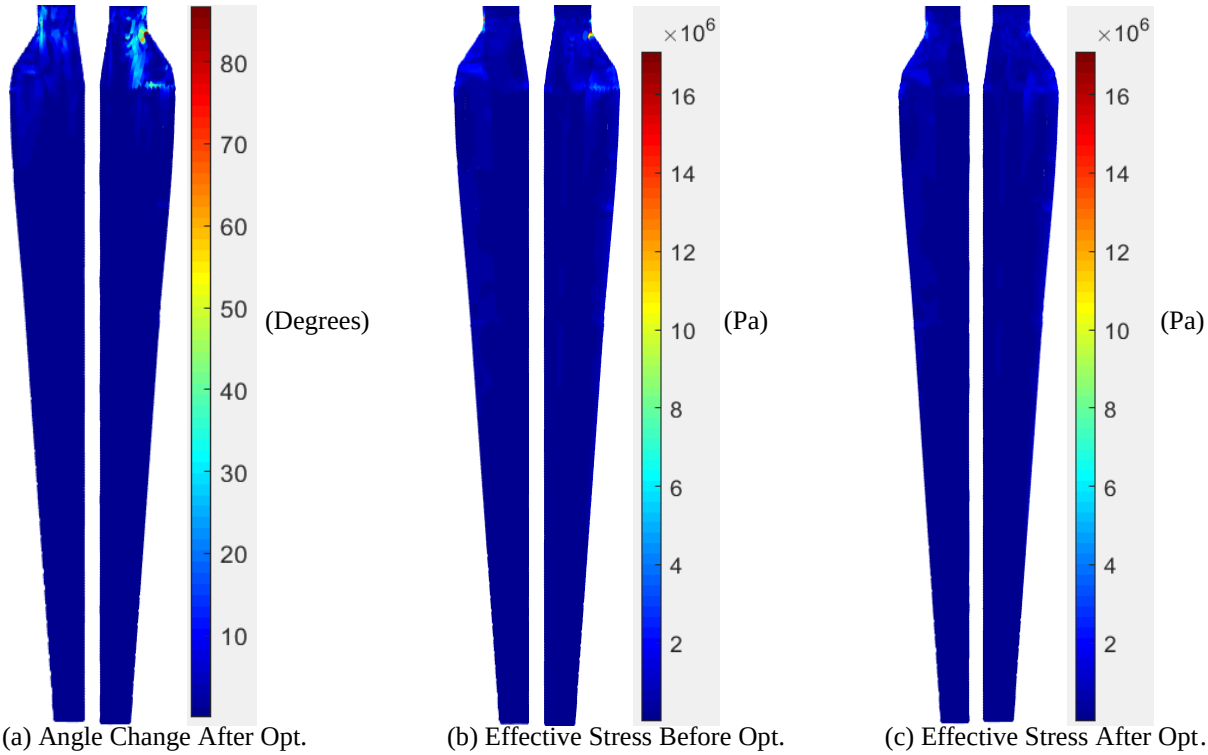

(a) Angle Change After Opt. (b) Effective Stress Before Opt. (c) Effective Stress After Opt.

Figure 8. Spatial distribution of local composite ply angle change and effective off-axis matrix stress before and after optimization for dynamic optimization subject to gravitational loads only.

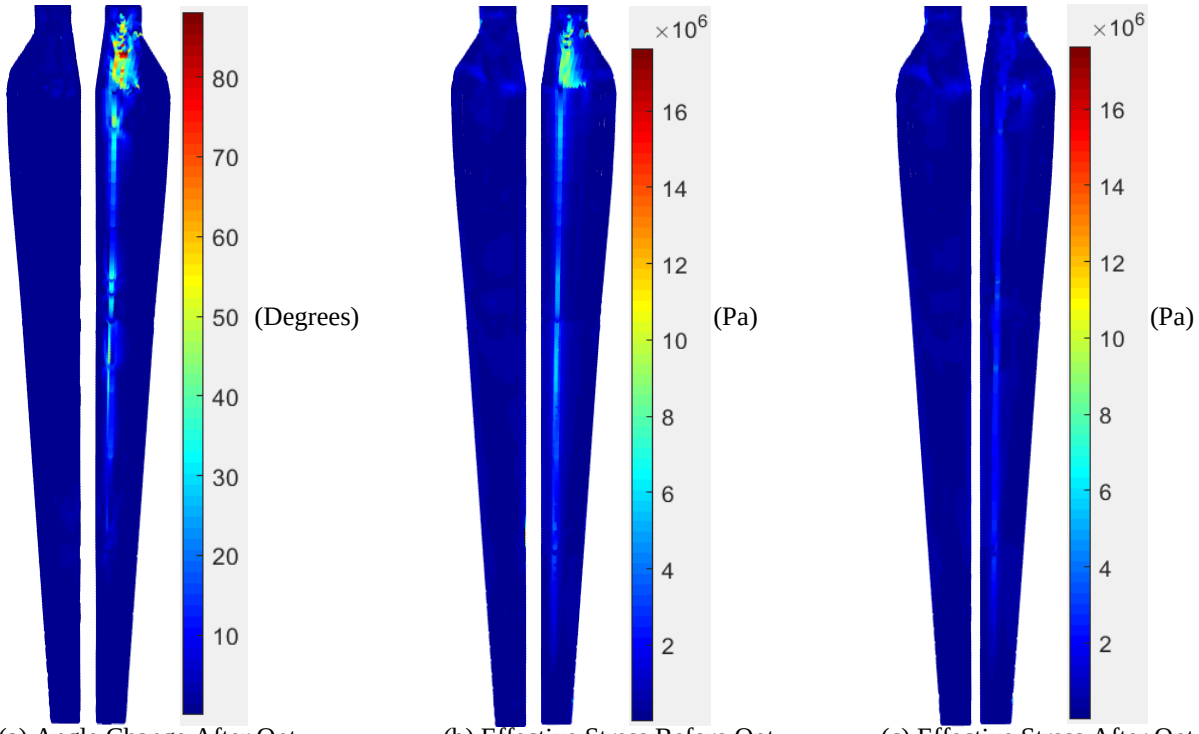

(a) Angle Change After Opt. (b) Effective Stress Before Opt. (c) Effective Stress After Opt.

Figure 9. Spatial distribution of local composite ply angle change and effective off-axis matrix stress before and after optimization for steady-state optimization subject to aerodynamic loads only.

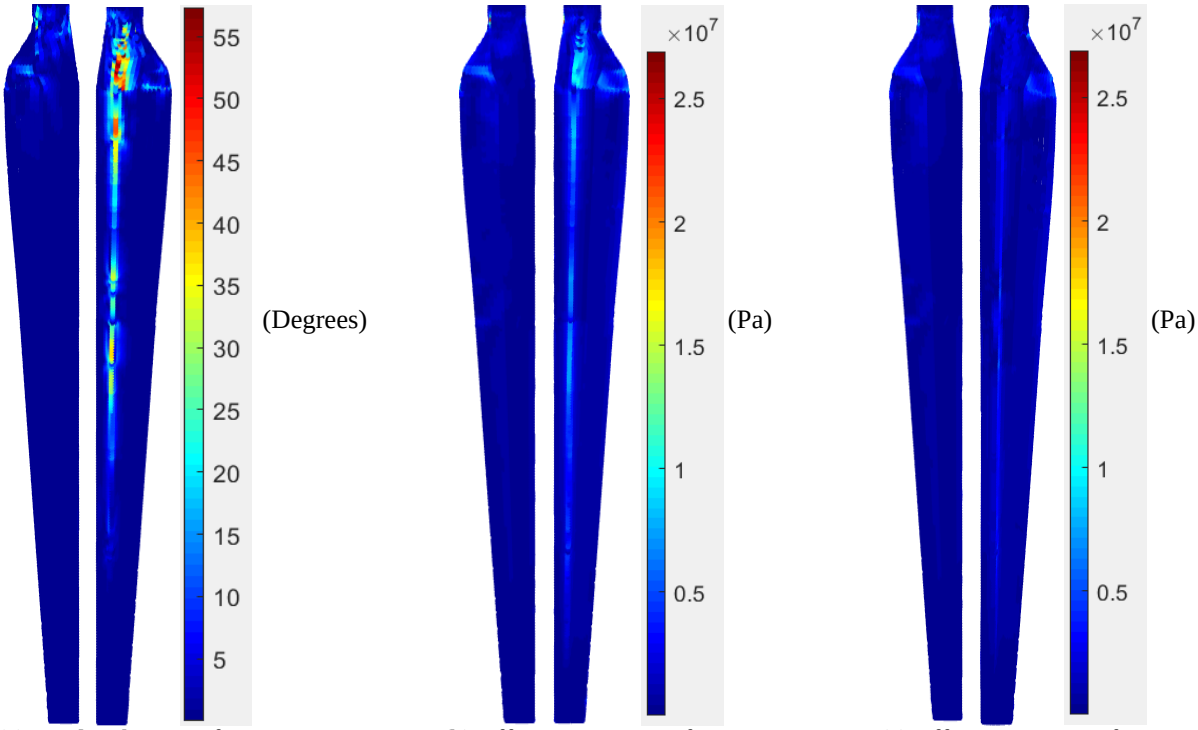

(a) Angle Change After Opt. (b) Effective Stress Before Opt. (c) Effective Stress After Opt.

Figure 10. Spatial distribution of local composite ply angle change and effective off-axis matrix stress before and after optimization for steady-state optimization subject to combined loading.

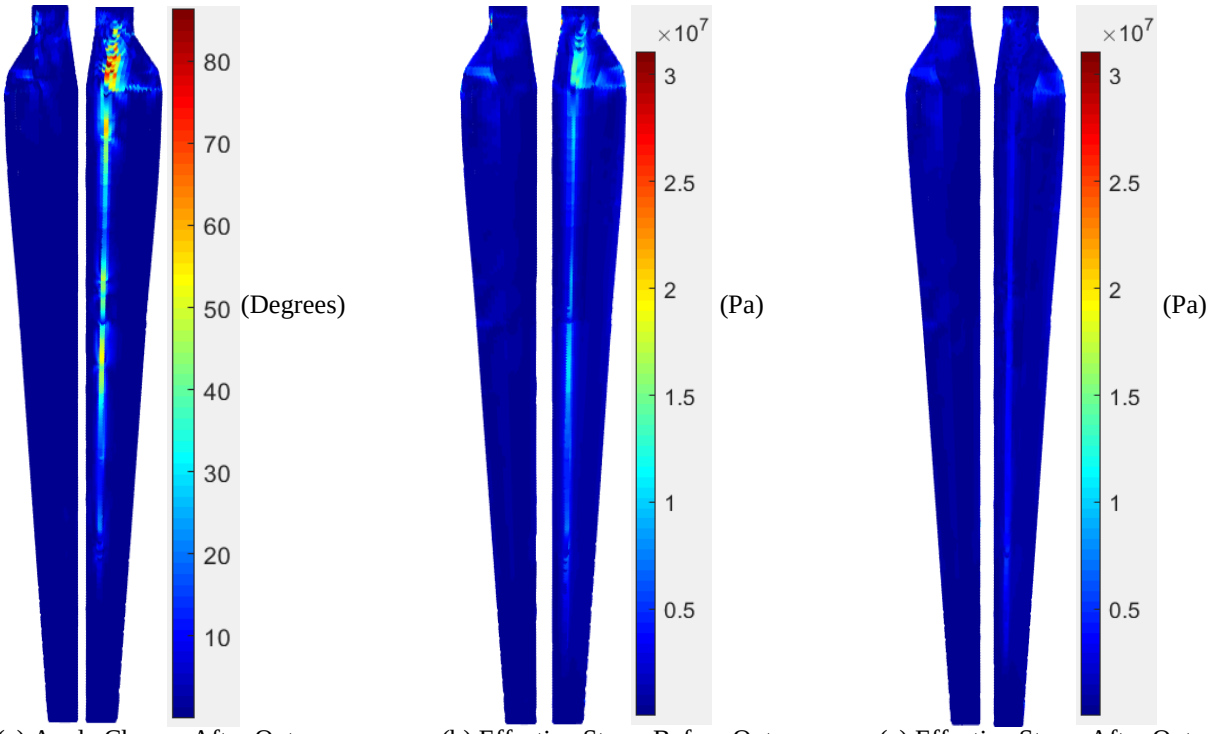

(a) Angle Change After Opt. (b) Effective Stress Before Opt. (c) Effective Stress After Opt.

Figure 11. Spatial distribution of local composite ply angle change and effective off-axis matrix stress before and after optimization for dynamic optimization subject to combined loading.

VI. Conclusions and Future Work

The present work can be thought of as an initial demonstration of the potential of adjoint-based structural optimization. The methods employed are computationally efficient, in this case requiring only a single desktop machine. Also the optimizations are evidently effective, seeing that in every optimization case the maximum fatigue-driving stress was reduced by at least 40%. Yet we have only scratched the surface of all that deserves to be investigated. The present optimization results indicate the potential to significantly improve fatigue life of wind turbine blades by only tailoring the composite ply configurations, without adding any mass, material cost or changing the external shape of the structure. However, we have assumed single-ply, unidirectional fiber composite makeup for every section of the blade, which is not accurate in practice. It is worth investigating further the effect of considering more realistic composite layups.

Our prediction of fatigue life improvement based on the S-N data trendline is optimistic, but is merely an estimation based on maximum values of off-axis matrix stress before and after optimization. An appropriate next step would be to perform a progressive failure fatigue analysis using the capability of Bhuiyan *et al.*[22] This would more thoroughly capture the evolution of damage from the actual states of stress in the blade, and give us a more accurate prediction of fatigue life.

Results under these conditions indicate that aerodynamic loads had the greatest influence on the optimal composite layup of the blade structure. This could be on account of the aerodynamic loads being primarily bending loads about the chord-direction, which generally lead to the highest stresses. However, the influence of gravitational and centrifugal loads were not drastically lower based on our metrics. Furthermore the SWiFT blade is relatively small at only 13 meters in length, and in general centrifugal and gravitational loads increasingly dominate the total loading experienced by a turbine blade as size increases. It would be of interest to investigate how the relative influence of each type of loading changes with increasing turbine size.

Although realistic aerodynamic loads generated by NSU3D were applied to the blade, the loads were for steady-state, idealized conditions, and were pre-generated before optimization. In reality wind blades regularly experience sudden gusts, which drastically increase loading and stresses on the blade. To truly capture this behavior, optimizations should be done with the fluid and structural solvers fully-coupled, simulating unsteady wind conditions while acconting for nonlinear geometric behavior. In this modeling environment, a blade's structural

properties could be tailored not only to reduce stress under a given load, but to allow the structure to adapt passively to varying wind conditions. This, along with the aforementioned follow-up studies are feasible goals for our aero-structural optimization capability in the years ahead.

VII. Acknowledgements

The authors wish to acknowledge the support for this work by the U.S. Department of Energy, Office of Science, Basic Energy Sciences, under Award DE-SC0012671, and by the University of Wyoming's College of Engineering and Applied Sciences Energy Graduate Assistantship.

References

[1]Hashin, Z. and Rotem, A., "A Fatigue Failure Criterion for Fiber Reinforced Materials," *Journal of Composite Materials,* Vol. 7, No. 4, 1973, pp. 448-464.

[2]Talreja, R., "Fatigue of Composite Materials: Damage Mechanisms and Fatigue-Life Diagrams," *Proceedings of the Royal Society of London A: Mathematical, Physical and Engineering Sciences.* 1981, The Royal Society.

[3]Coleman, B.D., "Time Dependence of Mechanical Breakdown Phenomena," *Journal of Applied Physics*, Vol. 27 No. 8, 1956, pp. 862-866.

[4]Regel, V., et al., "Polymer Breakdown and Fatigue," *Mechanics of Composite Materials,* Vol. 8, No. 4, 1972, pp. 516-527

[5]Tamuzh, V, "Fracture and Fatigue of Polymers and Composites (survey)," *Polymer Mechanics,* Vol. 13, No. 3, 1977, pp. 392-408.

[6]Sauer, J. and Richardson, G., "Fatigue of Polymers," *International Journal of Fracture,* Vol. 16, No. 6, 1980, pp. 499-532.

[7]Bhuiyan, Faisal H. and Fertig, Ray S. III., "A Physics-Based Combined Creep and Fatigue Methodology for Fiber-Reinforced Polymer Composites," *58th AIAA/ASCE/AHS/ASC Structures, Structural Dynamics, and Materials Conference, AIAA SciTech Forum,* 2017, p. 201.

[8]Fertig, R., "Bridging the Gap Between Physics and Large-Scale Structural Analysis: a Novel Method for Fatigue Life Prediction of Composites," *Proceedings of the SAMPE Fall Technical Conference*, 2009.

[9]Fertig III, R.S. and Kenik, D.J., "Predicting Composite Fatigue Life Using Constituent-Level Physics," 2011.

[10]Fertig, R. and Kenik, D., "Physics-Based Fatigue Life Prediction of Composite Structures," *NAFEMS World Congress 2011,* 2011.

[11]Resor, B. R. and LeBlanc, B., "An Aeroelastic Reference Model for the SWiFT Turbines," 2014, Sandia National Laboratories.

[12]Mavriplis, Dimitri, "Discrete Adjoint-Based Approach for Optimization Problems on Three-Dimensional Unstructured Meshes," *AIAA Journal,* Vol. 45, No. 4, April 2007.

[13]Mishra, Asitav, Mani, Karthik, Mavriplis, Dimitri and Sitaraman, Jay, "Time-Dependent Adjoint-Based Aerodynamic Optimization For Coupled Fluid-Structure Problems," *Journal of Computational Physics,* Vol. 292, 2015.

[14]Jameson, A., "Aerodynamic Shape Optimization Using the Adjoint Method," *VKI Lecture Series on Aerodynamic Drag Prediction and Reduction, von Karman Institute of Fluid Dynamics, Rhode St. Genese, Belgium,* 2003.

[15]Kenway, Gaetan K. W. and Martins, Joaquim R. R. A., "Multipoint High-Fidelity Aerostructural Optimization of a Transport Aircraft Configuration," *Journal of Aircraft,* Vol. 51, 2014, pp. 144-160.

[16]Mavriplis, D. J., Long, M., Lake, T., and Langlois, M., "NSU3D Results for the Second AIAA High-Lift Prediction Workshop," *AIAA Paper 2014-748 52nd Aerospace Sciences Meeting, National Harbor, MD.*

[17]Mavriplis, D., Anderson, E., Fertig, R. S., and Garnich, M., "Development of a High-Fidelity Time-Dependent Aero-Structural Capability for Analysis and Design," *57th AIAA/ASCE/AHS/ASC Structures, Structural Dynamics, and Materials Conference,* 2016, p. 1175.

[18]Mavriplis, D. J., Fabiano, E., and Anderson, E., "Recent Advances in High-Fidelity Multidisciplinary Adjoint-Based Optimization with the NSU3D Flow Solver Framework," *55th AIAA Aerospace Sciences Meeting,* 2017, p. 1669.

[19]Hilber, H. M., Hughes, T. J. R., and Taylor, R. L., "Improved Numerical Dissipation for Time Integration Algorithms in Structural Dynamics," *Earthquake Engng Struct. Dynamics,* Vol. 5, 1977, pp. 283-292.

[20]Abaqus, Version 6.14-4, product of Dassault Systemes Simulia Corp., 2017, Providence, RI, USA.

[21]Reddy, J.N., *Energy Principles and Variational Methods in Applied Mechanics*, John Wiley, 2002.

[22]Bhuiyan, Faisal Hasan, Mavriplis, Dimitri and Fertig, Ray S., "Predicting Composite Fatigue Life of Wind Turbine Blades Using Constituent-Level Physics and Realistic Aerodynamic Load," *57th AIAA/ASCE/AHS/ASC Structures, Structural Dynamics, and Materials Conference,* 2016, p. 988.

[23]Garnich, M. R. and Hansen, A. C., "A Multicontinuum Approach to Structural Analysis of Linear Viscoelastic Composite Materials," *Jounal of Applied Mechanics-Transactions of the ASME,* Vol. 64, No. 4, 1997, pp. 795-803.

[24]Garnich, Mark R. and Hansen, Andrew C., "A Multicontinuum Theory for Thermal-Elastic Finite Element Analysis of Composite Materials," *Journal of Composite Materials,* Vol. 31, No. 1, 1997, pp. 71-86.

[25]Nocedal, Jorge and Wright, Stephen, *Numerical Optimization,* Springer Science & Business Media, 2000.